Supporting Information

Polythiophene Side Chain Chemistry and its Impact on Advanced Composite Anodes for Lithium-Ion Batteries

Han Li,[1] Haoze Ren,[1] Zeyuan Sun,[1] Siyu Qin,[1] Armando Rodriguez Campos,[2,3] Esther S. Takeuchi,[2,3,4,5] Amy C. Marschilok,[2,3,4,5] Kenneth J. Takeuchi,[2,3,4,5] Elsa Reichmanis*[1]

[1] Department of Chemical and Bimolecular Engineering, Lehigh University, Bethlehem, PA, 18015, United States.

[2] Institute of Energy: Sustainability, Environment and Equity, Stony Brook University, Stony Brook, NY 11794.

[3] Department of Chemistry, Stony Brook University, Stony Brook, NY 11794.

[4] Department of Materials Science and Chemical Engineering, Stony Brook University, Stony Brook, NY 11794.

[5] Interdisciplinary Science Department, Brookhaven National Laboratory, Upton, NY 11973

*Corresponding Author: Elsa Reichmanis: elr420@lehigh.edu

Experimental Section

Materials

Fe_3O_4 nanoparticles (~10 nm) were synthesized by a previously reported coprecipitation process using an aqueous solution of iron (III) chloride hexahydrate, iron (II) chloride hexahydrate, and triethylamine.[1, 2] P3KBT (M_w: 19 kDa, polydispersity: 2.4, head to tail regioregularity: 89%), P3KPT (M_w: 28 kDa, polydispersity: 2.0, head to tail regioregularity: 89%), and P3KHT (M_w: 34 kDa, polydispersity: 2.3, head to tail regioregularity: 89%) were purchased from Rieke Metals Inc. PVDF (M_w: 90 kDa) was purchased from AME Energy (6020). Carbon black (Super P) was purchased from MTI. CR2032 coin cell shell was purchased from AME Energy. Lithium metal foil was purchased from Honzo Chemical Corp. 1 M LiPF6 in a mixture of ethylene carbonate (EC)/diethyl carbonate (DEC) (1:1 v/v %) was purchased from Sigma-Aldrich (746746).

Clarification on Fe_3O_4 Active Material

While magnetic contaminants can result in industrial processing issues in some cases, they can be intentionally removed as needed.[3] However, the magnetism of magnetite is not an issue with the processing method in this research. Here, magnetite was selected as a model insertion-conversion material with the opportunity for high theoretical capacity based on a green environmentally sustainable material, that is of considerable interest for lithium-ion batteries.[4, 5] From previous research,[5-8] use of P3KBT in composite metal oxide – based anodes significantly enhances the performance of Si, SiO and magnetite electrodes.

Electrode Fabrication

Composite electrode slurries were prepared by mixing Fe_3O_4 (0.14 g), Super P (0.03 g), and P3KBT/P3KPT/P3KHT in DI water (10 wt % solution, 0.3 g) or PVDF in N-methyl-2-pyrrolidone (5 wt % solution, 0.6 g) with a weight ratio of Fe_3O_4/carbon/polymer = 70:15:15. The 15 wt% carbon additive loading aligns with typical settings in academic research for exploring the properties of new electrode materials,[9] and in the range that has been reported for polythiophene-based binders that are reported to be able to reduce the need for carbon additives compared with conventional PVDF binders.[10] The active material mass loading was 0.9 – 1.3 g/cm^2. The composite electrodes were fabricated by the blade (purchased from MTI) coating the slurry onto the copper foil (purchased from MTI), and the samples were dried in the ambiance at room temperature for 1 h, followed by 110 °C for 12 h in a vacuum oven (purchased from Thermo Fisher Scientific, Model: 1326250) at 20 kPa. Pure polymer electrodes were prepared by spray coating aqueous solutions (2 mg mL^{-1}) of the respective polymers onto copper foil.

Electrochemistry

CR2032 coin cells (purchased from AME Energy) were used for electrochemical measurements. Lithium metal was used as a counter electrode, and 1 M $LiPF_6$ in ethylene carbonate (EC) and diethylene carbonate (DEC) (1:1 by weight) was adopted as electrolyte. The propylene membrane was used as a separator (Celgard 2400), and all assembly was

processed inside an argon filled glove box with moisture and oxygen content lower than 0.5 ppm. The as-assembled cells were stored in air overnight before measurement. For all electrochemistry characterizations, the C rate was calculated using the theoretical capacity of magnetite (926 mAh g^{-1})[4] and the active material composition (70 wt% of the electrode). The constant current measurement was operated using MZTC Multi-Chamber purchased from Arbin. Before electrochemical testing, all coin cells were charged and discharged at a rate of 0.01 C to conduct one formation cycle. The tests then proceeded for cycling and rate capability. All cycling performance (300 cycles) was conducted at a rate of 0.3 C in a voltage range of 0.01–3 V vs. Li/Li^+, whereas rate capability tests were conducted at varying charge and discharge rates (0.1, 0.3, 0.5, 1.0, and 2.0 C). Cyclic voltammetry (CV) was performed in the potential range of 0.01–3 V versus Li/Li^+ at scan rates of 0.1, 0.3, 0.5, 0.7, 1.0, 1.5, and 2.0 mV s^{-1}. Electrochemical impedance spectroscopy (EIS) measurements were conducted by PMC 200 purchased from AMETEK in the frequency range from 0.1 MHz to 0.1 Hz with open circuit potential as DC voltage and 10 mV root mean square (RMS) AC amplitude. Nyquist plots were fitted using ZView 3.

Microscopic Characterization

Surface and cross-sectional field-emission scanning electron microscopy (FE-SEM) images of the electrodes were obtained using a Hitachi 4300 SE/N FE-SEM with an accelerating voltage of 10 kV in the high vacuum mode at room temperature.

Spectroscopic Characterization

Fourier transform infrared (FT-IR) spectra were collected using a Thermo Scientific Nicolet iS50 FT-IR spectrometer. Data was collected from 750 cm^{-1} to 3500 cm^{-1} with a resolution of 0.4 cm^{-1}.

Supplementary Figures and Tables

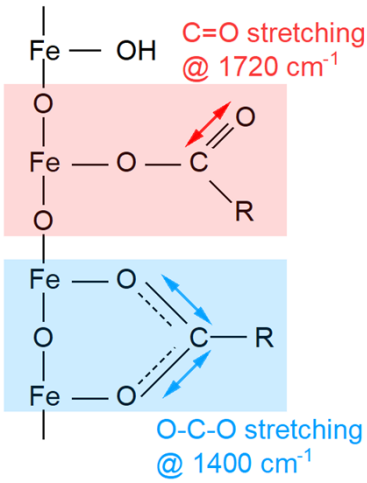

Figure S1. Possible chemical interactions between Fe_3O_4 and polymeric binders. Adapted from Kwon et al., *Chem. Mater*. 2016, *28* (18), 6689–6697. Copyright 2016 American Chemical Society.

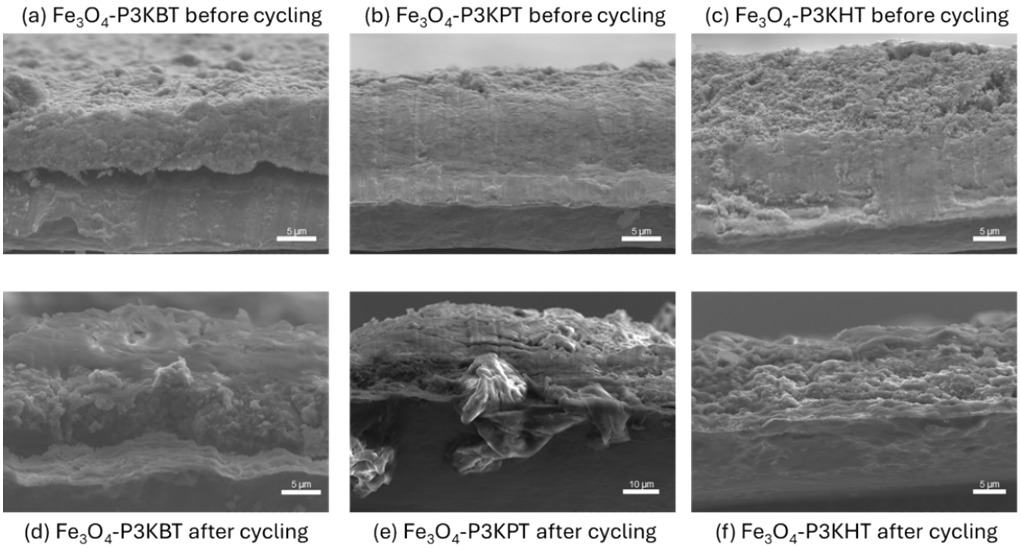

Figure S2. Cross-sectional view FE-SEM images of (a) Fe_3O_4-P3KBT, b) Fe_3O_4-P3KPT, (c) Fe_3O_4-P3KHT electrodes before cycling; and (d) Fe_3O_4-P3KBT, (e) Fe_3O_4-P3KBT, and (f) Fe_3O_4-P3KHT after cycling.

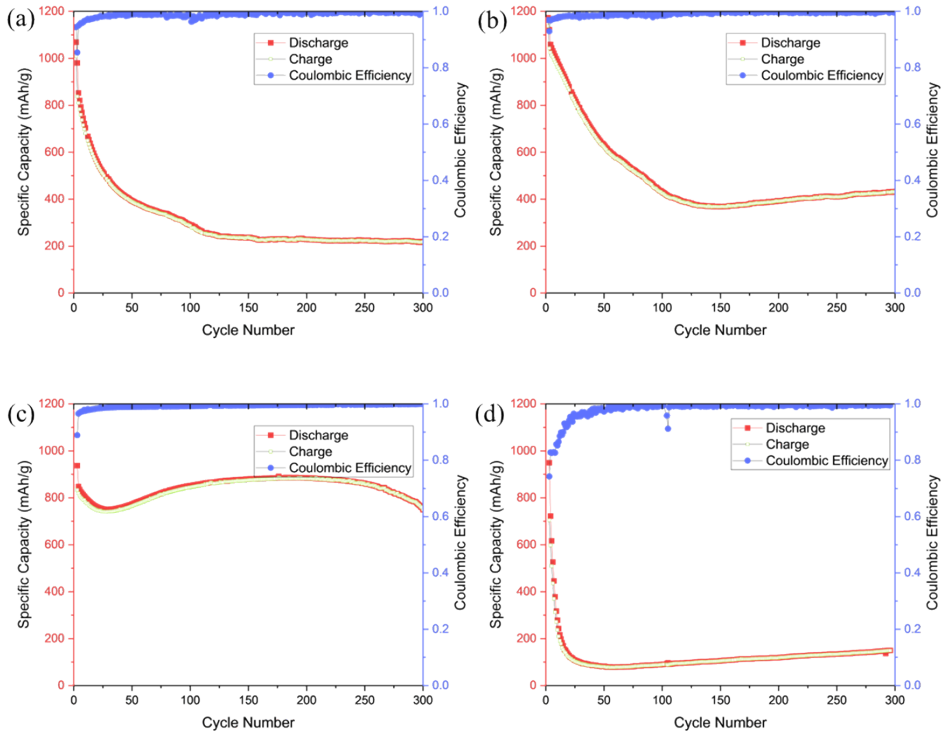

Figure S3. Cycling performance of Fe_3O_4 electrodes with different binder systems at 0.3 C between 0.01 and 3 V. (a) Fe_3O_4-P3KBT. (b) Fe_3O_4-P3KPT. (c) Fe_3O_4-P3KHT. (d) Fe_3O_4-PVDF.

In **Figure S3c**, an increase in capacity for Fe_3O_4-P3KHT samples during cycling is observed, even after an initial capacity drop in the first few cycles. This trend can be attributed to several potential factors. One possibility is the activation and reconstruction of the electrode materials during cycling, which is known to contribute to a gradual capacity increase in the transition of metal oxides. Another reason could be the pulverization of particles, leading to an enlarged surface area that provides more active sites for lithium storage and enhances catalytic activity.[11]

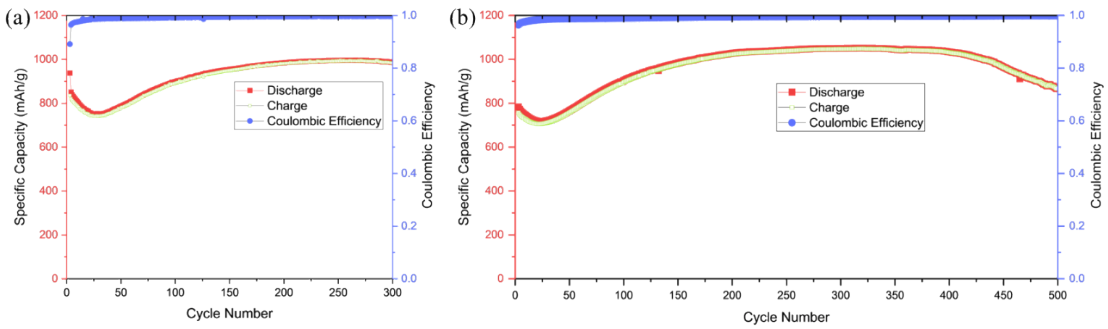

Figure S4. Cycling performance of Fe_3O_4-P3KHT electrodes at 0.3 C between 0.01 and 3 V for (a) 300 cycles and (b) 500 cycles.

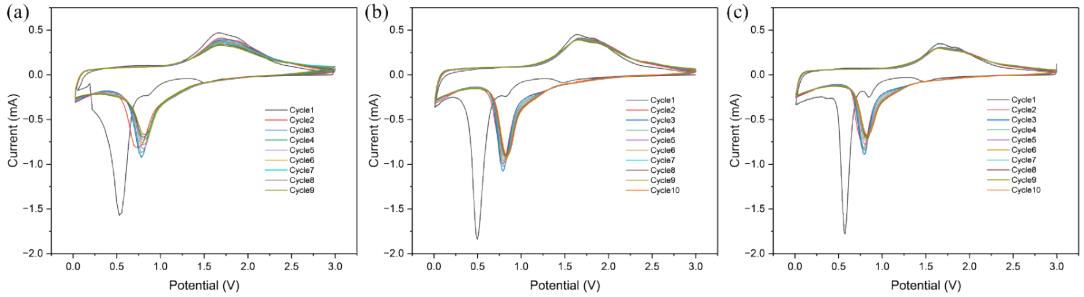

Figure S5. CV profiles of (a) Fe_3O_4-P3KBT, (b) Fe_3O_4-P3KPT, (c)Fe_3O_4-P3KHT electrodes in the potential window of 0.01 to 3 V versus Li/Li^+ (ten cycles) collected at the rate of 0.1 mV/s.

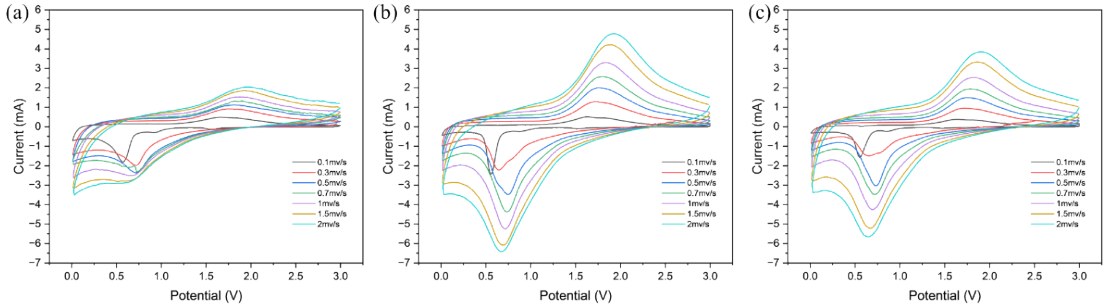

Figure S6. CV profiles with scan rates (v) in the range of 0.1 mv/s to 2 mv/s of (a)Fe_3O_4-P3KBT, (b)Fe_3O_4-P3KPT, and (c)Fe_3O_4-P3KHT in the potential window of 0.01 to 3 V versus Li/Li^+.

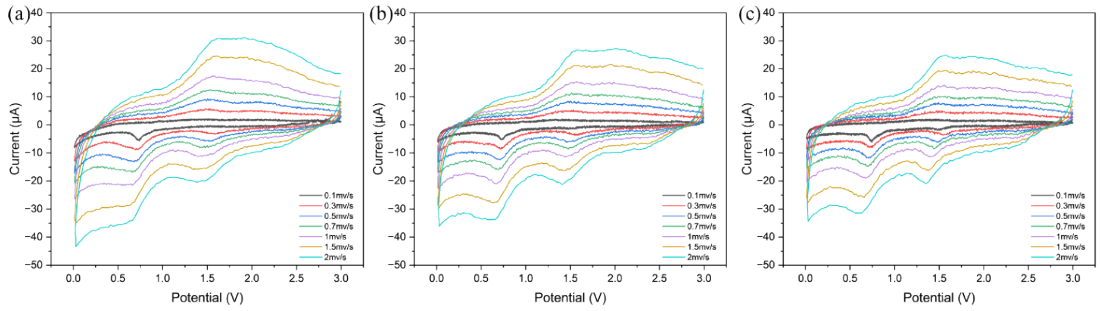

Figure S7. CV profiles with scan rates (v) in the range of 0.1 mv/s to 2 mv/s of (a) P3KBT, (b) P3KPT, and (c) P3KHT in the potential window of 0.01 to 3 V versus Li/Li^+.

Table S1. Fitting EIS results with Randles circuit model before cycling.

Before Cycling	Rs(Ω)	Rct(Ω)	Warburg Coefficient
Fe_3O_4-P3KBT	5.6	57.6	27.7
Fe_3O_4-P3KPT	9.1	56.2	14.8
Fe_3O_4-P3KHT	8.1	270.9	2.6
Fe_3O_4-PVDF	11.1	145.1	0.3

Table S2. Fitting EIS results with modified Randles circuit model after cycling.

After Cycling	Rs(Ω)	Rct(Ω)	R_{SEI}(Ω)	Warburg Coefficient
Fe_3O_4-P3KBT	12.3	48.8	69.5	2480.0
Fe_3O_4-P3KPT	8.8	55.9	9.2	6.1
Fe_3O_4-P3KHT	21.8	25.7	2.8	5.1
Fe_3O_4-PVDF	11.3	34.3	0.2	265.4

Table S3. The results of anodic peak currents of CV curves with different scan rates of P3KBT, P3KPT, and P3KHT.

Plot	**P3KBT**	**P3KPT**	**P3KHT**
Intercept	-0.955 ± 0.004	-0.878 ± 0.007	-1.070 ± 0.004
Slope	0.889 ± 0.013	0.862 ± 0.023	0.833 ± 0.013
Residual Sum of Squares	2.917×10^{-4}	9.625×10^{-4}	3.063×10^{-4}
Pearson's r	0.9996	0.9986	0.9995
R-Square (COD)	0.9992	0.9972	0.9991
Adj. R-Square	0.9990	0.9966	0.9988

Table S4. The results of anodic peak currents of CV curves with different scan rates of Fe_3O_4-P3KBT, Fe_3O_4-P3KPT, and Fe_3O_4-P3KHT electrodes.

Plot	Fe_3O_4-P3KBT	Fe_3O_4-P3KPT	Fe_3O_4-P3KHT
Intercept	-0.0627 ± 0.003	0.416 ± 0.011	0.358 ± 0.009
Slope	0.430 ± 0.008	0.694 ± 0.036	0.738 ± 0.031
Residual Sum of Squares	1.160×10^{-4}	2.440×10^{-3}	1.732×10^{-3}
Pearson's r	0.9993	0.9946	0.9966
R-Square (COD)	0.9987	0.9893	0.9932
Adj. R-Square	0.9983	0.9866	0.9916

References

1. S. Zhu, A. C. Marschilok, E. S. Takeuchi and K. J. Takeuchi, *Electrochemical and Solid-State Letters*, 2009, **12**, A91.
2. S. Zhu, A. C. Marschilok, E. S. Takeuchi, G. T. Yee, G. Wang and K. J. Takeuchi, *Journal of The Electrochemical Society*, 2010, **157**, A1158.
3. P. Ardia, S. Stallone and D. Cericola, *Talanta*, 2021, **224**, 121827.
4. A. M. Bruck, C. A. Cama, C. N. Gannett, A. C. Marschilok, E. S. Takeuchi and K. J. Takeuchi, *Inorganic Chemistry Frontiers*, 2016, **3**, 26-40.
5. H. Ren, H. Li, P. Barry, Z. Wang, A. R. Campos, E. S. Takeuchi, A. C. Marschilok, S. Yan, K. J. Takeuchi and E. Reichmanis, *Chem Mater*, 2024, **36**, 9299-9319.
6. Y. H. Kwon, K. Minnici, M. M. Huie, K. J. Takeuchi, E. S. Takeuchi, A. C. Marschilok and E. Reichmanis, *Chemistry of Materials*, 2016, **28**, 6689-6697.
7. Y. H. Kwon, K. Minnici, S. R. Lee, G. Zhang, E. S. Takeuchi, K. J. Takeuchi, A. C. Marschilok and E. Reichmanis, *ACS Applied Energy Materials*, 2018, **1**, 2417-2423.
8. R. Na, K. Minnici, G. Zhang, N. Lu, M. A. Gonzalez, G. Wang and E. Reichmanis, *ACS Appl Mater Interfaces*, 2019, **11**, 40034-40042.
9. J. Entwistle, R. Ge, K. Pardikar, R. Smith and D. Cumming, *Renewable and Sustainable Energy Reviews*, 2022, **166**.
10. N. Salem, M. Lavrisa and Y. Abu-Lebdeh, *Energy Technology*, 2015, **4**, 331-340.
11. S. Park, B. Seo, D. Shin, S. Chae, H. Cho, S. Kim and W. Choi, *Chemical Engineering Journal*, 2023, **470**.